The $^{10}B(\vec{p}, \gamma)^{11}C$ reaction at astrophysically relevant energies

A. P. Tonchev, S. O. Nelson, K. Sabourov, B. T. Crowley, K. Joshi, and H. R. Weller
Triangle Universities Nuclear Laboratory and Duke University, Durham, North Carolina 27708, USA

J. H. Kelley
TUNL and North Carolina State University, Raleigh, North Carolina 27695, USA

R. M. Prior and M. Spraker
North Georgia College and State University, Dahlonega, Georgia 30597, USA

N. Kalantar-Nayestanaki
KVI, Groningen, The Netherlands
(Received 23 April 2003; published 29 October 2003)

The $^{10}B(\vec{p}, \gamma)^{11}C$ reaction was studied by detecting the γ-rays produced when 100-, 130-, and 160-keV polarized protons were stopped in a thick ^{10}B target. Polarized and unpolarized incident beams were used to measure the cross section and vector analyzing power as a function of angle and energy for capture to the ground ($J^\pi=3/2^-$), the second ($E=4319$ keV, $J^\pi=5/2^-$), and the fifth ($E=6478$ keV, $J^\pi=7/2^-$) excited states of ^{11}C. The data were analyzed to obtain the amplitudes and phases of the contributing transition-matrix elements at each measured energy for all three transitions. Values of the astrophysical S factors were obtained from the cross section data and are compared to previous results. A direct capture plus resonance model calculation was performed in an attempt to account for all measured quantities. It was found that the large ($\sim$32%) value of $A_y(90°)$ observed in the case of capture to the ground state could be accounted for by including the subthreshold resonance at 8420 keV.

DOI: 10.1103/PhysRevC.68.045803 PACS number(s): 95.30.−k, 25.40.Lw

I. INTRODUCTION

Investigations of nuclear reactions induced by low-energy charged particles are important to nuclear astrophysics as well as to nuclear physics. Thermonuclear reactions for low-mass stars in hydrostatic equilibrium, like our sun, occur in the energy region around 10–30 keV. For more massive stars or for stars at more advanced stages in their evolution, ^{10}B can interact with cosmic ray protons. The $^{10}B(p, \gamma)^{11}C$ reaction is known to be involved in the nucleosynthesis of mass-11 nuclei. The production of ^{11}B, formed after β^+ decay of ^{11}C, provides one obvious example of how this could occur. In addition, the abundance ratio of ^{11}B to ^{10}B in the interstellar medium could be effected by stellar-nucleosynthesis processes such as the one described above.

Our previous studies of low-energy proton capture reactions using polarized protons have provided new insights into the reaction dynamics of proton capture processes at very low energies. It was, for example, the large analyzing power observed at 90° using 80 keV polarized protons which first indicated the presence of substantial p-wave capture in the $^7Li(p, \gamma)^8Be$ reaction [1]. Analyzing power data were also used to establish the parity of the 7.478 MeV state of ^{10}B; a result which affected the extrapolated S factor of the $^9Be(p, \gamma_0)^{10}B$ reaction by about 40% [2]. And a measurement of the analyzing powers in the $^{11}B(p, \gamma_1)^{12}C$ reaction using a 100-keV polarized proton beam was used to determine the relative phase of the resonance and direct-capture amplitudes involved in this reaction. This result led to a revised S factor for this reaction that was more than a factor of 2 greater than that previously determined [3].

The present study of the $^{10}B(p, \gamma)^{11}C$ reaction was motivated by the previously established effectiveness of polarized beam studies as a means for revealing the detailed nature of low-energy proton capture reactions, as described above. The goals of this work were to obtain a deeper insight into the reaction dynamics, and therefore a more reliable extrapolation of the astrophysical S factor for this reaction. Understanding the $^{10}B(p, \gamma)^{11}C$ reaction dynamics at very low energies presents problems of importance in both the nuclear and the astrophysical domains and therefore warrants a detailed study.

The existence of resonances in or near this low-energy region can drastically affect the reaction rate. This is the case for the $^{10}B(p, \gamma)^{11}C$ reaction where several resonances contribute to the low-energy behavior of the cross section. As was discussed in Ref. [4], there is an excited state in ^{11}C at $E_x=8699$ keV ($J^\pi=5/2^+$) which corresponds to an s-wave resonance at $E_R=10$ keV with $\Gamma_R=16$ keV. Due to this resonance, the cross section is greatly enhanced at low energies. As reported in Ref. [5], the measured value of the astrophysical S factor for the $^{10}B(p, \alpha)^7Be$ reaction increases by a factor of more than 200 as the energy decreases from $\sim$400 keV to 10 keV. Due to the importance of this energy range in nuclear astrophysics, it is worthwhile to establish a more detailed set of data for the $^{10}B(p, \gamma)^{11}C$ reaction. We have measured the cross section in the energy region overlapping that of Ref. [4] and extended the measurements to lower energies. In addition, polarized beam measurements have been carried out in order to more fully understand the mechanism of this proton capture reaction at these low energies.

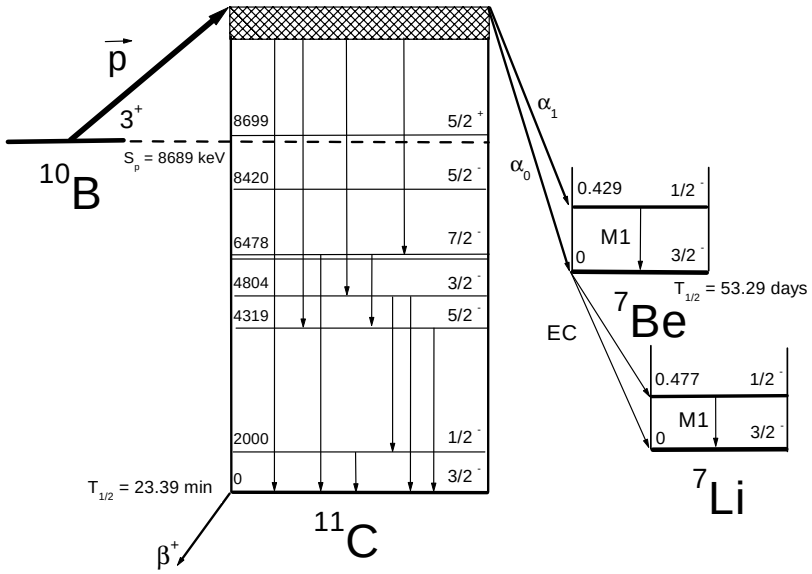

FIG. 1. Relevant energy levels of ^{11}C, ^{7}Be, and ^{7}Li following the ^{10}B$(p, \gamma)^{11}$C reaction.

The goal of this experiment was to extract the cross section and analyzing powers of the ^{10}B$(p, \gamma)^{11}$C reaction as a function of energy and angle from thick-target yields. In particular, the experimental γ-ray yields acquired with an unpolarized incident beam were used to calculate the cross section as a function of energy, $\sigma(E)$, and the corresponding astrophysical S factors. The γ-ray yields acquired with the polarized beam were used to obtain the vector analyzing power as a function of angle and energy, $A_y(\vartheta, E)$. Measurements were made at angles of 0, 25, 45, 60, 90, 135, and 150 deg for a proton energy 160 keV and at 0, 34, 90, and 126 deg for proton energies of 100 and 130 keV.

II. LEVEL PROPERTIES OF ^{11}C

Figure 1 shows some of the relevant nuclear levels of ^{11}C, ^{7}Be, and ^{7}Li populated in the ^{10}B$(p, \gamma)^{11}$C reaction. The ground state of ^{11}C is known to have $J^{\pi}=3/2^{-}$,$T=1/2$, and is rather long lived ($T_{1/2}$=23.39 min) decaying by positron emission to ^{11}B. According to the shell model, the ground state is essentially a pure $p_{3/2}$ single-particle state with a spectroscopic factor of 1.09 [6]. After proton capture, γ decay is also observed to the second excited state (4.319 MeV and $J^{\pi}=5/2^{-}$), which subsequently decays to the ground state. The second excited state is considered a mixture of $p_{3/2}$ (0.0964) and $p_{1/2}$ (0.0388) single-particle states. The fifth excited state is 6.478 MeV above the ground state. This state is also considered a mixture of single particle states $p_{3/2}$ and $p_{1/2}$ with the spectroscopic factors of 0.0539 and 0.8230, respectively. Protons incident on ^{10}B can also proceed via the ^{10}B$(p, \alpha)^{7}$Be reaction which dominates over the ^{10}B$(p, \gamma)^{11}$C reaction. In addition, the (p, α) channel can lead to the first excited state of ^{7}Be at 429 keV, which γ decays to the ground state. The ground state of ^{7}Be is radioactive with a half-life of 53.3 days and decays with 10.52% by electron capture to the first excited state in ^{7}Li. The emitted γ ray for decay of this level to the ground state of ^{7}Li has an energy of 477 keV.

By simultaneously measuring the γ rays from the ^{10}B$(p, \alpha_1\gamma)^{7}$Be reaction and the γ rays from ^{10}B$(p, \gamma)^{11}$C, one can determine the cross section of the ^{10}B$(p, \gamma)^{11}$C reaction from the previously measured cross sections of the ^{10}B$(p, \alpha_1)^{7}$Be reaction [7].

III. EXPERIMENTAL PROCEDURE

Measurements of the yields from the ^{10}B$(\vec{p}, \gamma)^{11}$C reaction for capture to the ground, second, third, and fifth excited states of ^{11}C were carried out at the Triangle Universities Nuclear Laboratory (TUNL). In this section, detailed descriptions of the beam, targets, and γ-ray detectors used in this experiment are presented.

A. Proton beam and thick target

The polarized proton beam from the TUNL atomic beam polarized ion source (ABPIS) has a maximum beam energy of 80 keV. To increase the effective beam energy to 160 keV, a −80 kV bias was applied to the target chamber, which was attached to the beam line with a multisection acceleration tube. A measurement of the beam current integration was not possible due to the strongly biased target. The polarization state of the incident proton beam was flipped (at 10 Hz) between the spin-up and the spin-down configurations. The beam polarization was measured using the spin-filter polarimeter [8], with typical values of (80±0.03)%.

Targets enriched to 99.8% in ^{10}B with a thickness of 1.7 (0.2) μm and diameters of 2.5 cm were used. These targets were produced by evaporating the enriched boron onto a tantalum backing (1 mm thick) [9]. The proton beam was collimated with a thin (0.1 mm) stainless steel collimator having an aperture of 1.5 cm located 10 cm before the ^{10}B target.

Stopping the beam completely in the target created a range of incident proton beam energies between the incident proton beam energy and zero. Consequently, this range of incident beam energies creates a corresponding range of outgoing γ-ray energies, which leads to a broadening of the γ-ray spectral lines.

B. HPGe efficiency and attenuation corrections

Four identical high-purity germanium (HPGe) detectors with efficiencies of 60% each relative to a standard 3″ ×3″ NaI detector were mounted 8 cm from the ^{10}B target. With that setup it was possible to measure four data points in the angular distribution at a given incident energy. In a second run, three of the detectors were rotated around the target. The fourth detector remained in the same position (θ=150 deg) as in the first run. The angles of the detectors with respect to the proton beam were 0, 25, 45, 60, 90, 135, and 150 deg. A 123% HPGe detector was used with an unpolarized proton beam. The data with this detector were taken at 90 deg with proton beam energies of 100, 120, 130, and 160 keV.

Because the γ rays measured in this experiment were spread over a broad energy range, from 0.430 MeV to almost 9 MeV, knowledge of the efficiency curve of HPGe as well as attenuation coefficients for the target chamber walls at these γ energies were very important. Hence the relative efficiencies of the HPGe detectors were obtained by measuring the photopeak efficiency for the E_γ ranging from 1.77 to 10.7 MeV produced by the $^{27}Al(p, \gamma)^{28}Si$ resonance at E_R =992 keV. A 997-keV proton beam from the TUNL FN tandem accelerator was stopped in a 0.2-mm Al target on a 0.8-mm-thick Cu backing. Utilizing the E_R=992 keV resonance from the $^{27}Al(p, \gamma)^{28}Si$ reaction for the efficiency calibration has two main advantages: the γ rays arising from the $^{27}Al(p, \gamma)^{28}Si$ reaction have a wide energy range from 1.77 to 10.7 MeV and the intensities are well studied [10]. The γ rays produced from the resonance were observed with two (60% and 123%) HPGe detectors, positioned at θ=45 and 90 deg at distances of 19.5 cm and 14.5 cm from the end of the aluminum target, respectively; 3 h of collecting data with an average beam current of 300 nA allowed us to obtain statistical uncertainties in the photopeak area of 0.5–5 % for the strongest branches. A plot of the data obtained from the $^{27}Al(p, \gamma)^{28}Si$ reaction is shown along with the data obtained using a calibrated ^{226}Ra source in Fig. 2. The ^{226}Ra source covers the energy range from 0.180 to 2.4 MeV, which overlaps the data obtained with the $^{27}Al(p, \gamma)$ reaction. The solid line represents a fit to these data using the MCNP Monte Carlo code [11]. The energies of the simulations were chosen to be the same as these of the γ transitions in ^{28}Si and ^{226}Ra. The calculated detector efficiencies were in very good agreement with the predictions of the MCNP calculations over the entire energy region (0.180 MeV$<E_\gamma<$10.7 MeV).

All measured γ-ray yields were corrected for attenuation through the stainless steel target chamber (6.35-mm-thick) and Plexiglas (1.0-cm-thick) shielding. From 0.1 to 2.4 MeV the experimental values for the attenuation coefficients were obtained using a ^{226}Ra source. Measuring the relative intensities of the γ lines of this source in the position of the target, with and without the chamber, allowed us to determine the total attenuation coefficients up to 2.4 MeV. At higher energy this information was obtained from a simulation using MCNP.

The background was reduced by placing 10 cm of passive Pb shielding around the HPGe detectors. In order to minimize the effect of the high counting rate on the data acquisition system for 429-keV γ rays, produced by the $^{10}B(p, \alpha_1)^7Be$ reaction and, after some irradiation time, the 477-keV γ rays emitted in the 53-day γ decay of ^7Be, a 0.3-cm-thick lead absorber was placed between the target and the detectors. The 429-keV line was observed for two purposes. First, the S factor for the $^{10}B(p, \gamma)^{11}C$ reaction can be normalized to the $^{10}B(p, \alpha_1)^7Be$ reaction by measuring the 429-keV decay line to the ground state of ^7Be. Second, this line also provided information on the intensity of the beam and the quality of the target. When the count rate coming from the 429-keV γ line dropped by 20% from its initial value, the ^{10}B target was replaced.

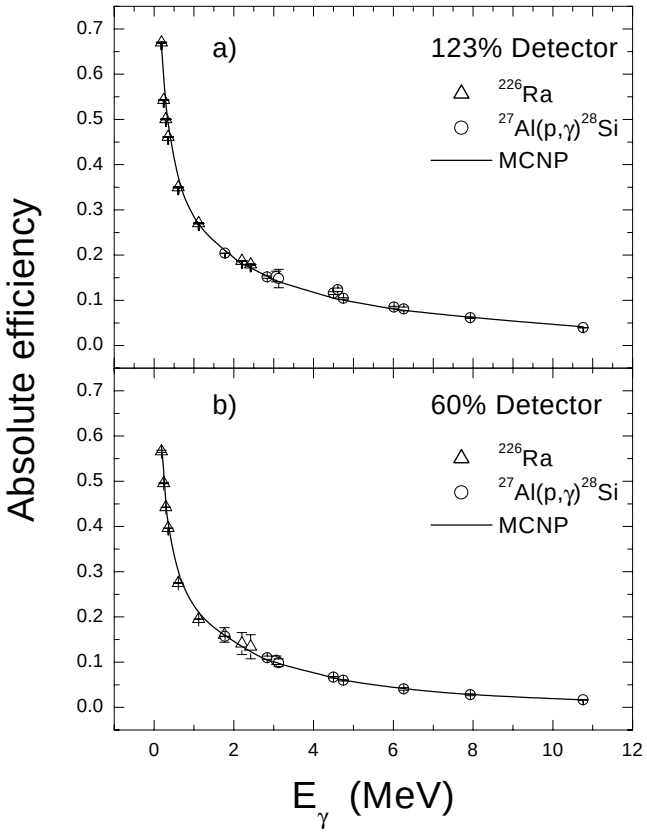

FIG. 2. Experimental intrinsic photopeak efficiency curve for the 123% (a) and 60% (b) HPGe detectors. The open circles are the experimental data obtained from the $^{27}Al(p, \gamma)^{28}Si$ reaction and the open triangles were taken from ^{226}Ra source. The solid lines are the results of an MCNP simulation (see text).

A typical γ-ray spectrum for the reaction $^{10}B(p, \gamma)^{11}C$ at E_p=160 keV and θ=90 deg is shown in Fig. 3. Intensity distributions from spin-up- and spin-down states are presented for four regions of the γ-ray spectrum. In Fig. 3(a) 429-keV line represents the γ line stemming from the $^{10}B(p, \alpha_1)^7Be$ reaction. In Fig. 3(b) the peak at 4510 keV represents the primary transition to the second excited state (J^π=5/2$^-$) and the peak at 4319 keV is its subsequent transition to the ground state. Figure 3(c) shows the full energy peak, and the single escape peak (SEP) for the transitions from the fifth excited state (J^π=7/2$^-$) to the ground state. The full energy peak at E_γ=8824 keV in Fig. 3(d) is 45 keV wide and corresponds to capture to the ground state (J^π=3/2$^-$). This width arises because the 160-keV proton beam is

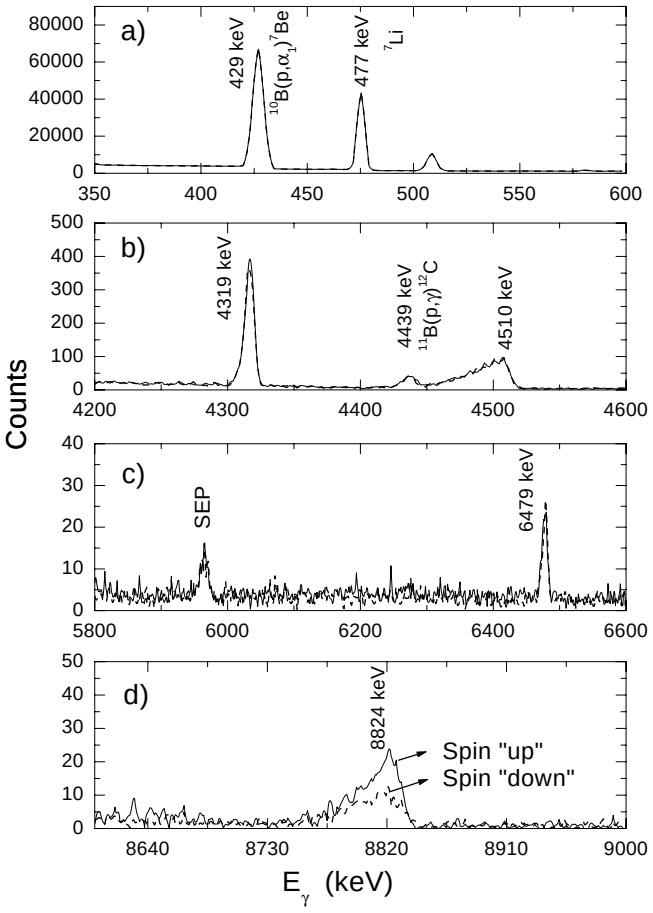

FIG. 3. HPGe spectrum for the $^{10}B(p, \gamma)^{11}C$ reaction taken at a lab angle of 90 deg. Four energy regions of the spectrum are shown: (a) 429-keV line stemming from the $^{10}B(p, \alpha_1)^7Be$ reaction, (b) the proton capture to the second excited state, (c) the secondary transition to the fifth excited state, and (d) the capture to the ground state. The solid line labels spin state "up" while the dotted line is for spin state "down."

stopped in the thick ^{10}B target. It should be pointed out that in Figs. 3(a)–3(c) there are no differences in the intensity distributions between the spin-up and spin-down state. However, for the capture to the ground state, the spin-up state shows 57% more net counts than observed for the spin-down state.

C. Data analysis

In order to determine the *S* factor of the $^{10}B(p, \gamma)^{11}C$ reaction, the measured reaction yield was compared with the yield of the $^{10}B(p, \alpha_1)^7Be$ reaction, which is measured in the same experiment. As has been mentioned in the preceding section, the intensity of the 429-keV line, corresponding to the decay of the first excited state in ^7Be to the ground state, is proportional to the $^{10}B(p, \alpha_1)^7Be$ cross section. The *S* factor of the (p, α_1) reaction was previously measured in Ref. [7]. The ratio of photopeak areas of the (p, γ) and (p, α_1) reactions can be written as

$$\frac{N_{p,\gamma}}{N_{p,\alpha}} = \frac{\varepsilon_{p,\gamma} A_{p,\gamma} Y_{p,\gamma}(E_p)}{\varepsilon_{p,\alpha} A_{p,\alpha} Y_{p,\alpha}(E_p)}, \tag{1}$$

where ε is the detector efficiency for the corresponding γ line and *A* is the attenuation factor for a given γ line. The yield of the proton capture reaction is given by

$$Y(E_p) = \int_{E_p}^{0} \sigma(E)/\mathrm{STP}(E) dE, \tag{2}$$

where STP(*E*) represents the stopping power of the ^{10}B target. However, the cross section at projectile energies below the Coulomb barrier decreases exponentially with decreasing beam energy. To extrapolate the data to the very low energies relevant to astrophysics, it is advantageous to transform the cross section into the astrophysical $S(E_{\mathrm{c.m.}})$ factor defined by the relation [12]

$$\sigma(E_{\mathrm{c.m.}}) = \frac{S(E_{\mathrm{c.m.}}) \exp(-2\pi\eta)}{E_{\mathrm{c.m.}}}, \tag{3}$$

where η is the Sommerfeld parameter and $E_{\mathrm{c.m.}}$ is center-of-mass energy in keV. The quantity η is related to the center-of-mass energy as follows:

$$\eta = \frac{31.29 Z_1 Z_2}{2\pi} \sqrt{\frac{\mu}{E_{\mathrm{c.m.}}}}, \tag{4}$$

where Z_1 and Z_2 are the charge numbers of the interacting nuclei and μ is the reduced mass in amu. Substituting Eq. (3) into Eq. (2) and Eq. (2) into Eq. (1), we obtain

$$\frac{N_{p,\gamma}(E_p)}{N_{p,\alpha}(E_p)} = C \frac{\int_{E_p}^{0} \frac{S_{p,\gamma}(E) e^{-2\pi\eta}}{E\ \mathrm{STP}(E)} dE}{\int_{E_p}^{0} \frac{S_{p,\alpha}(E) e^{-2\pi\eta}}{E\ \mathrm{STP}(E)} dE}, \tag{5}$$

where the constant *C* is the ratio of the detector efficiencies and attenuation coefficients for the (p, γ) and (p, α_1) reactions, respectively. The available data [13] show that the angular distribution of the γ rays is isotropic at the relevant low energies for the (p, γ) and $(p, \alpha\gamma)$ reactions, and this was assumed in the present analysis. The functional form used to describe the energy distribution of the astrophysical factor for both $(p, \alpha\gamma)$ and (p, γ) channels are polynomials of second degree and are given by

$$S(E_{\mathrm{c.m.}}) = S_0 + S_1 E_{\mathrm{c.m.}} + S_2 E_{\mathrm{c.m.}}^2, \tag{6}$$

where S_0, S_1, and S_2 are parameters determined from the fit, and $E_{\mathrm{c.m.}}$ is in keV. As will be shown in the following section, these three parameters for the $(p, \alpha\gamma)$ reaction were obtained by fitting the experimental data from Ref. [7]. Consequently, the uncertainty in the value of the *S* factor for the (p, γ) reaction depends on the uncertainties in the detector efficiencies, the attenuation coefficients, and the *S* factor for the (p, α_1) reactions. Since we assume a polynomial distribution of second order for the form of the *S* factors for both the (p, γ) and the (p, α_1) reactions, a system of at least three linear equations is required in

order to unambiguously determine the S_0, S_1, and S_2 parameters for the (p, γ) reaction. In the present analysis, data at four different incident proton energies have been used to determine the parameters of the S factor, which makes the system of linear equations completely determined.

D. Legendre fit

Based on the formalism presented in Ref. [14], the vector analyzing power is defined as

$$A_y(\theta, E) = \frac{Y_+(\theta, E) - Y_-(\theta, E)}{p_y^- Y_+(\theta, E) + p_y^+ Y_-(\theta, E)}, \tag{7}$$

where Y_+ and Y_- denote the number of events from the $^{10}B(p, \gamma)^{11}C$ reaction with the spin polarized along the spin-up and spin-down directions, respectively, and p_y^+ and p_y^- denote the polarizations of the beam for the two different proton spin states. A fit to Legendre and associated Legendre polynomials was performed on the $\sigma(\theta, E)$ and $\sigma(\theta, E)A_y(\theta, E)$ data at each energy. The vector analyzing power $A_y(\theta, E)$ relates the polarized beam cross section σ_p to the unpolarized cross section σ_u in terms of the vector polarization of the beams, p_y, by

$$\sigma_p(\theta, E) = \sigma_u(\theta, E)[1 + p_y A_y(\theta, E)]. \tag{8}$$

The cross section can be written in terms of Legendre polynomials as

$$\sigma(\theta, E) = A_0\left[1 + \sum_{k=1}^{n} a_k Q_k P_k(\cos\,\Theta)\right]. \tag{9}$$

The product of the cross section and the analyzing powers can be written in terms of associated Legendre polynomials as

$$\sigma(\theta, E)A_y(\theta, E) = A_0 \sum_{k=1}^{n} b_k Q_k P_k^1(\cos\,\theta), \tag{10}$$

where the Q_k are the finite geometry attenuation factors, a_k and b_k are the coefficients of the normalized Legendre polynomials P_k and P_k^1, the Legendre and first associated Legendre polynomials, respectively. A_0 is the absolute cross section normalization constant:

$$\sigma_t = 4\pi A_0. \tag{11}$$

IV. EXPERIMENTAL RESULTS

A. *S*-factor determination

The absolute cross section of the reaction $^{10}B(p, \alpha_1\gamma)^7Be$ has been previously reported at effective energies of E =48–159 keV [5,7]. Figure 4 shows these data for the astrophysical S factor from the reaction $^{10}B(p, \alpha_1)^7Be$, as a function of center of mass energy (open circles). The S factor exhibits a strong energy dependence at very low-energies due to the low energy resonance at E_p=10 keV. For this reason a quadratic function was used in the present analysis in order to represent the energy dependence of the experimental data from Ref. [7] in the range from 50 to 160 keV. The smooth curve presented in Fig. 4 is the result of a χ^2 minimization fit to the data points. The functional form used in this case is a polynomial of second degree and is given by Eq. (6). The values of the S_0, S_1, and S_2 coefficients are 405.8±38.7 keV b, −4.8±0.7 b, and 0.016±0.003 keV^{-1} b, respectively, and the χ^2 from the fit is 0.94 per degree of freedom. If the E^2 term is not included, the χ^2 per degree of freedom is 1.31, indicating the necessity of using a polynomial of second degree.

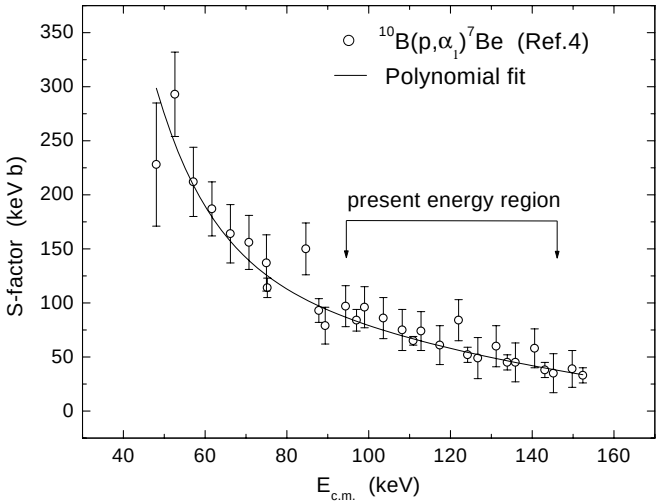

FIG. 4. Astrophysical S factor as a function of center-of-mass energy. The solid line is the second-order polynomial fit to the experimental data [7].

In the present experiment, measurements of the 429-keV γ transition from the $^{10}B(p, \alpha_1\gamma)^7Be$ reaction have been used to determine the S factor and the cross section for the $^{10}B(p, \gamma)^{11}C$ reactions by direct normalization. The astrophysical S factors for the $^{10}B(p, \gamma)^{11}C$ reaction have been determined from four measurements of the ratio $N_{p,\gamma}/N_{p,\alpha}$ of Eq. (5) performed at beam energies of E_p=160, 130, 120, and 100 keV, corresponding to c.m. energies of 145 keV, 118 keV, 109 keV, and 91 keV. These were used to generate four simultaneous versions of Eq. (5) in the three unknowns S_0, S_1, and S_2. Results were obtained for the three strongest transitions: capture to the ground state, to the second exited state, and to the fifth excited state. These results are presented in Table I. The experimental errors of the S-factor values are mainly determined by uncertainties in the measured γ rays from the (p, γ) reaction [(3–10)%], the relative γ-ray efficiencies (±2%), and the attenuation coefficiencies (±2%). All transitions to the ground, the second, and the fifth excited states show the same behavior: all of them have negative slopes. The energy dependence of the S factor was extracted from our data and found to rise by a factor of 7, 4, and 7 for the capture to the ground, second, and fifth excited states, respectively, as the energy is decreased from $E_{c.m.}$ =145 to 91 keV. These results are all summarized in Table I.

B. Analyzing power

The measurement of the analyzing power for the $^{10}B(\vec{p}, \gamma)^{11}C$ reaction, $A_y(\theta, E)$, was performed using the po-

TABLE I. *S*-factor data for the reaction $^{10}B(p,\gamma)^{11}C$.

Coefficient	*S* factor (keV b) Ground state $J^\pi=3/2^-$	Second excited state $J^\pi=5/2^-$	Fifth excited state $J^\pi=7/2^-$
S_0 (keV b)	16.38±0.53	15.93±0.37	3.59±0.04
S_1 (b)	−0.25±0.01	−0.22±0.01	$(-0.05\pm6)\times10^{-4}$
S_2 (keV^{-1})	$9.64\times10^{-4}\pm3.85\times10^{-5}$	$8.30\times10^{-4}\pm2.81\times10^{-5}$	$2.14\times10^{-4}\pm2.69\times10^{-6}$

larized proton beam from the ABPIS. The positive *y* axis was defined as $\vec{k_{in}}\times\vec{k_{out}}$, where $\vec{k_{in}}$ is the direction of the incident proton beam and $\vec{k_{out}}$ is the direction of the outgoing γ ray. For the case of a detector on the left side of the beam line, the spin quantization axis corresponds to the $+y$ direction.

The primary advantage associated with measuring the vector analyzing power is that it depends only on the ratio of yields, not on the absolute magnitude of the yields themselves. This means that the measuring of A_y, unlike the cross section, does not require any knowledge of the stopping powers or relative detector efficiency and attenuation. The flipping of the spin state every third of a second ensured similar experimental conditions for each spin state. As a result, A_y can be expected to be independent of the systematic errors which are present in cross section measurements.

The experimental analyzing powers, measured at three proton energies, are shown in Fig. 5. A_y was obtained by comparing the yields for spin-up and spin-down states within the same gate. This gate was set to the photopeak and first escape peak of the ground, first, and fifth excited states. The background, which was fitted using a second order polynomial was subtracted from each peak and was less than 1% of the total photopeak area.

It can be seen from Fig. 5 that the analyzing power for capture to the ground state is nonzero and shows a maximum at 90 deg for all three energies. In addition, this distribution is symmetric around 90 deg. It is also seen that the maximum value of $A_y(90\text{ deg})$ is 0.32 for $E_p=160$ keV and drops to 0.22 at $E_p=100$ keV. Unlike the transition to the ground state, the analyzing powers to the second ($J^\pi=5/2^-$) and fifth ($J^\pi=7/2^-$) excited states are consistent with zero to within error. This picture demonstrates that in addition to the influence of the $E1$ *s*-wave resonance, the proton capture to the ground state is governed by a significant *p*-wave component since pure $E1$ radiation would give $A_y(90\text{ deg})=0.0$.

C. Transition-matrix element analysis

The angular distribution of the cross section and the analyzing power can provide further information on the reaction via the extraction of transition matrix elements (TMEs) [15]. This analysis provides a model-independent determination of the amplitudes and phases for the individual channels. The procedure used here is to vary the amplitudes and phases of the TMEs to fit the data, while searching for a minimum in the χ-squared.

In order to determine the appropriate TMEs to be considered for the $^{10}B(p,\gamma)^{11}C$ reaction, the angular momentum and parity of the constituent particles need to be examined. The incident proton and ^{10}B target have spin and parities of $1/2^+$ and 3^+, respectively. For the ground state capture, the ^{11}C ground state has $J^\pi=3/2^-$, and for the capture to the second and fifth excited states, $J^\pi=5/2^-$ and $J^\pi=7/2^-$, respectively. At the low energies of the current experiment, *s*-wave $E1$ and *p*-wave $M1$ radiations are expected to dominate. So, in the present analysis we neglect all γ transitions higher than dipole. The diagram in Fig. 6 shows the four dipole transitions, labeled by the quantum numbers S, ℓ, J of the incident channel and the multipolarity for the $^{10}B(p,\gamma_0)^{11}C$ reaction. Since the ^{11}C ground state has a negative parity, the

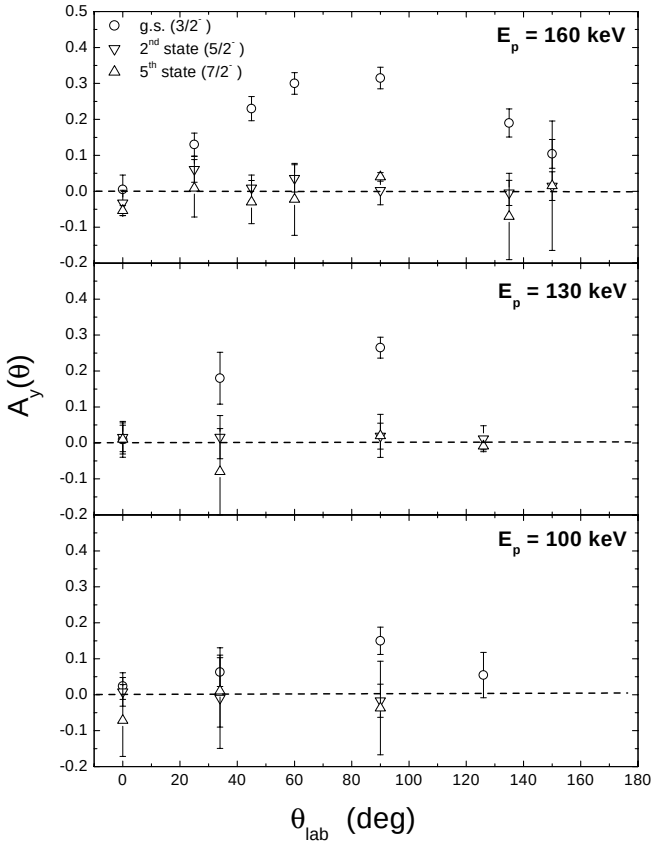

FIG. 5. The angular distribution of the analyzing power at $E_p=100$, 130, and 160 keV for the $^{10}B(p,\gamma)^{11}C$ reaction leading to the ground state (○), the second excited state (▽), and the fifth excited state (△). The errors bars represent the statistical uncertainties associated with the data point and the uncertainty in the beam polarization.

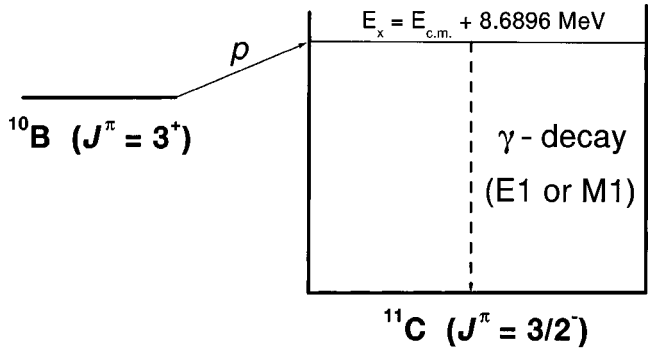

1. S = 5/2	$\ell = 0$	$J^\pi = 5/2^+$ (E1)
2. S = 5/2	$\ell = 1$	$J^\pi = 3/2^-$ (M1)
3. S = 5/2	$\ell = 1$	$J^\pi = 5/2^-$ (M1)
4. S = 7/2	$\ell = 1$	$J^\pi = 5/2^-$ (M1)

FIG. 6. The ^{10}B-p system captures into a ^{11}C continuum state ($E_x \sim E_{c.m.}+Q$) which then decays labeled by γ emission. The four dipole TMEs to the ground state are shown by the quantum numbers S, l, and J, and by the multipolarity of the outgoing γ ray.

s-wave ($\ell=0$) continuum states decay via $E1$ radiation while the p-wave ($\ell=1$) continuum states decay via $M1$ radiation.

Equations (8) and (10) were fit simultaneously to the angular distribution data of the analyzing power and the cross section, and the a_k and b_k coefficients were extracted from these fits. The results of the Legendre polynomial fit to the cross section (a_1 and a_2) and vector analyzing power (b_1, b_2) are displayed in Fig. 7 and listed in Table II. It can be seen here that a_1 and a_2 are nonzero only for the ground state case. The other two cases are consistent with the assumption of isotropy (straight-line fit) since a_1 and a_2 are statistically consistent with being equal to zero. The physical significance of this is that an isotropic $\sigma(\theta)$ is predicted for the case of pure s-wave capture. The b_1 coefficient, which by Eq. (10) arises from $E1$-$M1$ mixing, is consistent with zero for the capture to the second and fifth excited states, while for capture to the ground state it reaches a value of 0.31. The b_2 coefficient is consistent with zero for all three states. The χ^2/ν for the overall TME fits are given in Table III.

A T-matrix element analysis was performed using the one $E1$ and three $M1$ matrix elements listed in Fig. 6. To determine a unique solution, both the one $E1$ and the three $M1$ matrix elements were treated as free parameters with all of the $M1$ TME phases set to be equal to one another. A χ^2 minimization routine was applied to both the cross section and analyzing power data simultaneously. Table III shows the numerical results of the TME analysis for the $^{10}B(p, \gamma)^{11}C$ for the s-wave $E1$ amplitude, the p-wave $M1$ amplitude, the fraction (%) and the relative phase (deg), and the χ-squared per degree of freedom (χ^2/ν). The transition-

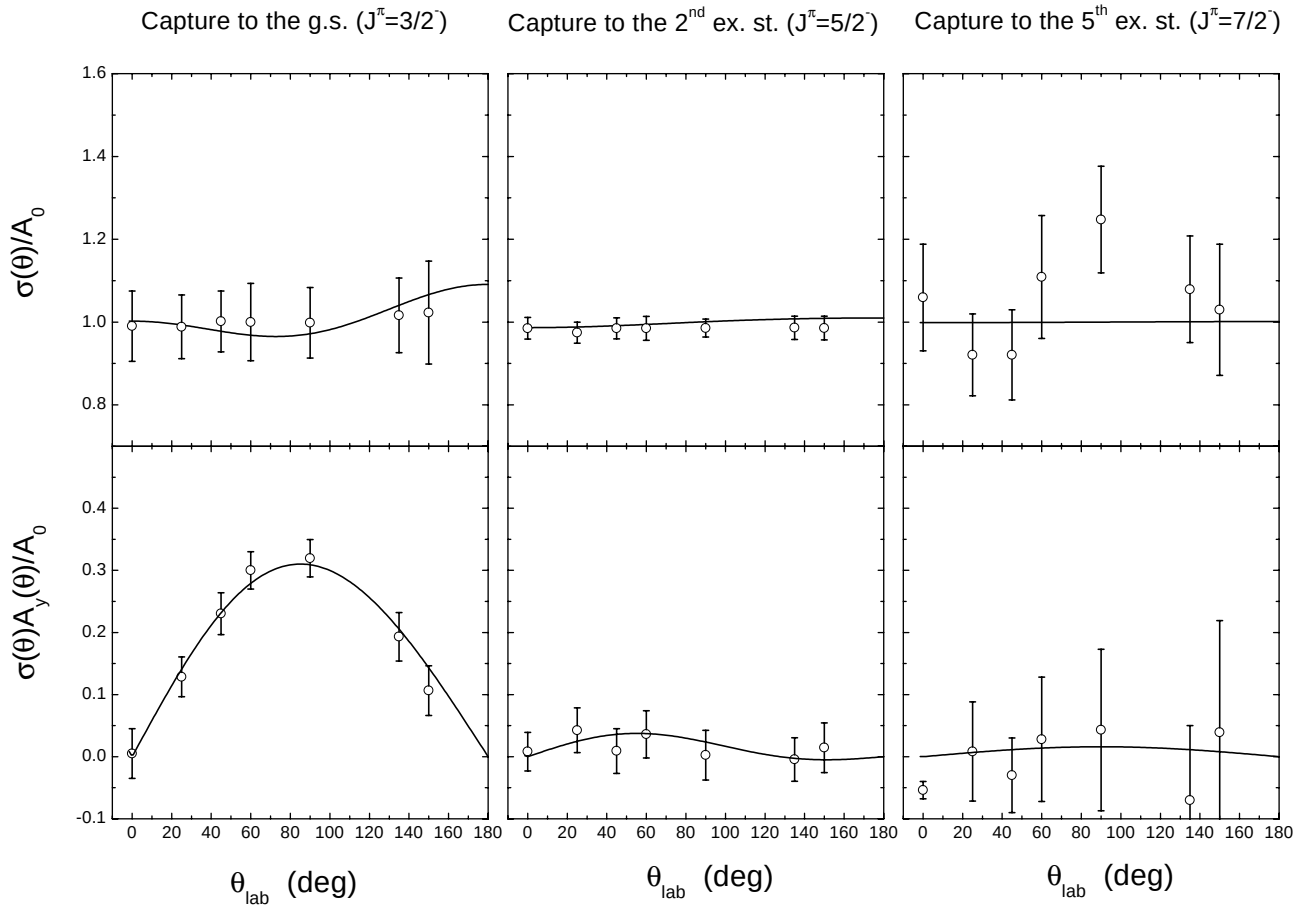

FIG. 7. The experimental data for the reaction $^{10}B(p, \gamma_0, \gamma_2, \gamma_5)^{11}C$ at E_p=160 keV. The solid lines are the results of a simultaneous fit to both observables in terms of the TMEs [see Eqs. (8) and (10)].

TABLE II. Results of Legendre polynomial fit. Coefficients for the fits to the cross section (a_1 and a_2) and vector analyzing power (b_1 and b_2) are presented for the proton capture to the ground state ($J^\pi=3/2^-$), second ($J^\pi=5/2^-$), and fifth ($J^\pi=7/2^-$) excited states.

	$E_{\text{c.m.}}=132$ keV		
Coefficient	Ground state $J^\pi=3/2^-$	Second state $J^\pi=5/2^-$	Fifth state $J^\pi=7/2^-$
a_1	-0.044 ± 0.041	-0.012 ± 0.475	-0.07 ± 0.12
a_2	0.050 ± 0.034	$-1.7\times10^{-5}\pm4\times10^{-5}$	$4.3\times10^{-4}\pm2\times10^{-4}$
b_1	0.309 ± 0.037	0.024 ± 0.036	-0.008 ± 0.01
b_2	0.0	0.0	0.0

matrix elements are expressed as the percent contribution to the total cross section. The phases are relative to the $E1$ term that has been set arbitrarily to zero. The TME analysis indicates that 87% of the cross section at $E_p=160$ keV arises from $E1$ s-wave radiative capture while the rest is due to the $M1$, p-wave capture. In Table III, the $M1$ contribution is the sum of all three $M1$ transitions to the ground state. The fraction of the cross section due to the $J^\pi=3/2^-$ $M1$ amplitude (see Fig. 6) is $(12.3\pm2.23)\%$, while for the second and third $J^\pi=5/2^-$ $M1$ contributions these numbers are $(0.2\pm0.63)\%$ and $(0.5\pm0.21)\%$, respectively. Hence, the p-wave capture to the ground state is dominated more than 95% by the $J^\pi=3/2^-$ $M1$ p-wave term. At the same time, the radiative capture transition to the second and fifth excited states are dominated (more than 99%) by $E1$, s-wave capture. After excluding the second and third $M1$ amplitudes, the analysis shows that the relative phases between the $E1$ and $M1$ TMEs is 86 ± 3.2 deg, which is in very good agreement with the point charge Coulomb phase shift value (86.4 deg) [16].

Figure 7 shows the relative cross section $[\sigma(\theta)/A_0]$ and analyzing power $[\sigma(\theta)A_y(\theta)/A_0]$ data for proton capture to the three final states at $E_p=160$ keV. We also notice from Fig. 7 that the transition-matrix element fit does a fairly good job of representing the angular distribution at all measured energies, indicating that the assumptions made in the TME analysis were reasonable.

V. DIRECT-CAPTURE-PLUS-RESONANCE CALCULATION

In order to understand the origin of the analyzing power observed in the present experiment, a series of direct $E1$ and $M1$ capture plus $E1$ and $M1$ resonance calculations were performed using the computer program HIKARI [17]. In these calculations, single-particle resonance amplitudes for the dipole transitions are added to the amplitudes.

The radial part of the electric dipole transition amplitude T_{fi}, for the direct-capture process, is given by

$$T_{fi}=\langle\Psi_f|\varepsilon r|\Psi_i\rangle, \tag{12}$$

where Ψ_i is the initial elastic-scattering state wave function, Ψ_f is the single-particle component of a final bound state, ε is the dipole effective charge of the proton, and r is the form of the electric dipole operator in the long-wavelength approximation. The initial wave function is calculated from a Woods-Saxon potential, where the parameters are taken from optical model fits to elastic scattering [18]. The radial wave function of a final single-particle state is determined by adjusting the depth of a Woods-Saxon potential so as to reproduce the proton binding energy. The resulting resonance parameters along with the other parameters of the calculation are given in Table IV. The excitation energies and widths for these resonances were taken from Ref. [4]. As has been mentioned in the Introduction, at low energies ($E_p<0.6$ MeV) there are two s-wave resonances at $E_p=0.010$ and 0.56 MeV. The analyzing power for capture to the ground state has a value of 0.32 at 90 deg. A finite analyzing power at 90 deg requires the presence of radiations of opposite parities. In Ref. [4] it was shown that only strong, destructive interference between the $E_p=0.01$ and 0.56 MeV resonance can fit the low energy structure of the S factor curve. However, s-wave $E1$ resonances alone cannot reproduce the observed analyzing powers. The only way to produce a large analyzing power at 90 deg in the ground state channel is to have a spin-parity of $3/2^-$ or

TABLE III. TME fit for the reaction $^{10}\text{B}(p,\gamma)^{11}\text{C}$ at $E_{\text{c.m.}}=145$ keV. Partial wave contributions to the cross section for the transition to the ground, second, and fifth excited states in ^{11}C via polarized proton capture as predicted by a TME analysis. The χ^2/ν values are given for each fit.

			Ground state $J^\pi=3/2^-$		Second excited state $J^\pi=5/2^-$		Fifth excited state $J^\pi=7/2^-$	
ℓ_{in}	J^π_{CN}	TME	Fraction (%)	Phase (deg)	Fraction (%)	Phase (deg)	Fraction (%)	Phase (deg)
0	$5/2^+$	$E1$	87 ± 3	0.0 (Fixed)	99.9 ± 0.6	0.0 (Fixed)	99.6 ± 2.3	0.0 (Fixed)
1	$3/2^-$	$M1$	13 ± 2	86.0 ± 3.2	0.1 ± 0.09	76.0 ± 21	0.04 ± 0.06	134 ± 121
	χ^2/ν		0.576		0.536		1.988	

TABLE IV. The parameters used to calculate the analyzing power and S factors for $^{10}B(p,\gamma)^{11}C$. The energy and the resonance parameters are given in the center-of-mass frame.

Final state (J^π)	Spectroscopic factor	Excitation energy (MeV)	Single-particle state	J^π	Resonance parameters E_R (keV)	Γ_{tot} (keV)	$\omega\gamma$ (keV)
Ground ($3/2^-$)	1.09	8.699	$^1p_{3/2}$	$5/2^+$	9±1.0	15±1	8.0×10^{-22}
Second ($5/2^-$)	0.0964	4.83	$^1p_{3/2}$	$5/2^+$	509±55	500±100	3.1 ± 10^{-55}
	0.0388	4.83	$^1p_{1/2}$	($3/2^-$)	955±55	210±50	3.3×10^{-4}
Fifth ($7/2^-$)	0.0539	6.48	$^1p_{3/2}$	($5/2^-$)	1091±45	240±60	1.8×10^{-4}
Subthreshold	0.39	8.420	$^1p_{1/2}$	$7/2^-$	−265.0	0.0000154	

$5/2^-$ contributing $M1$ strength. Our transition-matrix analysis also indicates that $M1$-$E1$ interference is the origin of the large analyzing power observed in the case of capture to the ground state. Besides direct $M1$ strength, there are two types of states that can contribute to the $M1$ strength: the first ones are the conjectured high lying resonances with spin and parities of $3/2^-$ (E_x=9.65 MeV) and $5/2^-$ (E_x=9.78 MeV) [19], which can $M1$ decay to the ground state after p-wave proton capture. The second is the $M1$ contribution from the weakly bound subthreshold state at an excitation energy of 8.420 MeV ($J^\pi=5/2^-$). We would like to explore these possibilities.

A direct-capture-plus-resonance calculation was performed by simultaneously fitting the S factor or cross section data and the analyzing power data at the measured proton energies. These calculations were adjusted to best represent all of the data presented in Fig. 8. The results indicate that the two p-wave $M1$ resonances at 9.65 and 9.78 MeV can yield a maximum of A_y(90 deg) of 0.20 compared to the observed value of ~0.32. The results of these calculations are shown in Fig. 8. The other possible source for the missing analyzing power is the weakly bound, $5/2^-$ subthreshold state at 8.42 MeV. This $M1$ strength could interfere with the direct $E1$ strength in order to produce the observed value of A_y(90 deg).

The resonance parameters used in the present calculation to fit the S factor as shown in Fig. 8 are presented in Table IV [4]. The resonance strengths were adjusted to fit simultaneously the analyzing power data and the low-energy part of the S-factor data ($E_p<1.3$ MeV). Increasing the strength of the subthreshold resonance can increase the analyzing power from a value of 0.20 at E_p=160 keV to the experimental values of 0.32. At this strength, the direct-capture-plus-resonance calculation fit both the S factor and the analyzing power data reasonably well. It has to be mentioned that the subthreshold state has a negligible impact on the S-factor data at very low energies, since the S factor in this region is completely dominated by the $E1$ resonance at E_p=10 keV. Our calculation shows, for example, that in the vicinity of this resonance the cross section coming from this resonance is more than four orders of magnitude higher than the cross section from the p-wave $M1$ resonances. Experimental data for the analyzing power together with HIKARI calculations are shown in Fig. 9 for proton energies of 100 and 130 keV. As can be seen, the calculation is in very good agreement with experimental data. At the same time, the analyzing power at 16 keV is zero, which is expected due to the dominance of the s-wave $E1$ resonance at E_R=10 keV.

The strength of the subthreshold state which reproduced the observed A_y(90 deg) can be expressed in terms of the spectroscopic factor (C^2S) of the 8.420 MeV state. To do this we used the previously reported γ width Γ_γ and wrote the proton particle width as C^2S times the proton penetrability with the reduced width taken to be equal to the Wigner limit.

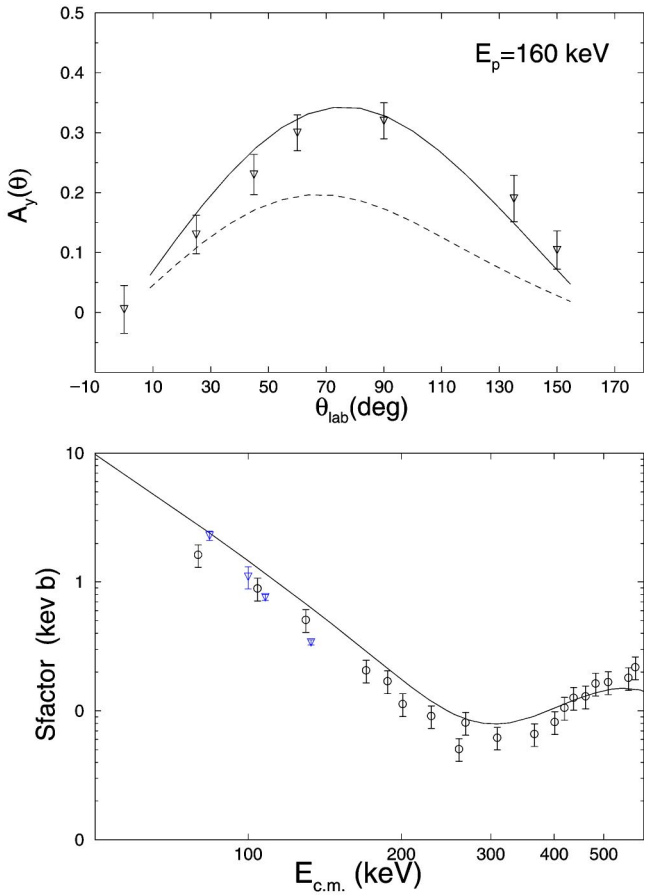

FIG. 8. Experimental and calculated (a) analyzing power obtained at E_p=160 keV (E_{eff}=132 keV) and (b) S factor for the radiative proton capture to the ground state ($J^\pi=3/2^-$) in ^{11}C. Triangles are the present experimental data and the open circles are the data from Ref. [4]. The solid lines represent calculations for the direct-plus-resonance calculation performed at an effective energy of 132 keV. The dotted line is the same calculation when the subthreshold state is not included. The results in this case for the S factor are indistinguishable from the solid curve.

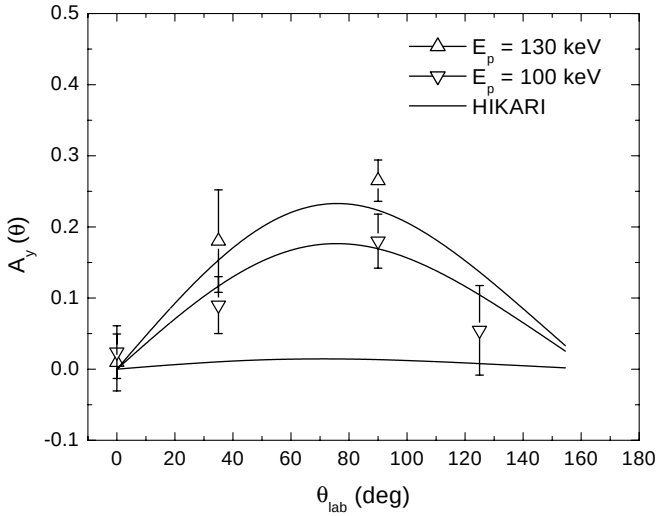

FIG. 9. Analyzing power at E_p=130 (E_{eff}=108 keV) (△) and 100 keV (E_{eff}=84 keV) (▽). HIKARI calculations are presented with continuous lines. The calculations were performed at effective energies of 108 and 84 keV, respectively. The lowest curve shows the results of the calculation at E_p=16 keV.

$$\Gamma_p(E) = 2P_l(E, R_N)C^2S\left(\frac{\hbar^2}{\mu R_N^2}\right). \tag{13}$$

Then, with $\Gamma=\Gamma_p+\Gamma_\gamma$, we find that C^2S=0.42. This value is in good agreement with the value of 0.39±0.4 obtained from a previous direct-capture experiment [4].

Combining the analyzing power and the cross section data allows a deeper understanding of the reaction mechanism in the low-energy region. This information is valuable to understand the interplay between the two major transition-matrix elements $E1$ and $M1$. The calculated values of A_y(90 deg) and the cross section ratio of the $M1$ versus $E1$ transitions, resulting from HIKARI calculation, is shown in Fig. 10. Figure 10 (a) shows that the A_y(90 deg) increases as the proton energy increases, reaching a maximum value of about 0.46 at $E_{\text{c.m.}}$=245 keV. The area around 245 keV coincides with the minimum in the S factor as shown in Fig. 8. This calculation also reproduces the present A_y(90 deg) data at the three effective energies as shown in Fig. 9. The effective energy corresponds to that energy within the target at which one-half of the reaction yield is obtained [12]. Calculation shows that at $E_{\text{c.m.}}$=245 keV the $M1$ cross section becomes almost equal to the $E1$ cross section [see Fig. 10(b)]. As reported in Ref. [4], there is strong destructive interference between the first two $E1$ resonances. As can been seen in Fig. 10(b), there is also strong distructive interference between the $E1$ and $M1$ components, giving rise to the large analyzing powers in this energy region above 100 keV. At $E_{\text{c.m.}}$=145 keV the calculated value of the ratio of the $M1$ versus $E1$ cross sections is 0.12, which is in good agreement with the results of the transition-matrix element analysis (0.13).

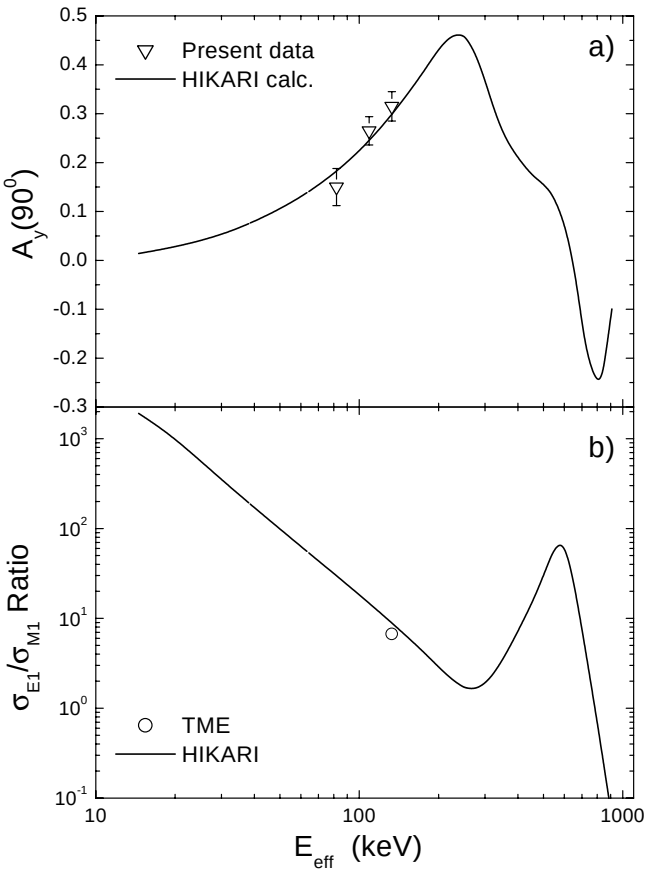

FIG. 10. Energy dependence of the analyzing power and the ratio of the $E1$ vs $M1$ cross section calculation. The present data for A_y(90 deg) are shown in (a), and the result of our TME analysis is shown at $E_{\text{c.m.}}$=132 keV in (b).

VI. THE REACTION RATE OF THE ^{10}B(p, γ)^{11}C REACTION

The reaction rate $N_A\langle\sigma v\rangle$ was calculated taking into account the experimental data from Refs. [4,20] and the present experimental data at E_p below 160 keV as represented by the parameters of Table I. Together, these data cover the region from E_p=0.1 to 17 MeV. In the energy range below $E_p<90$ keV, no experimental data are available, so for $1<E_p<16$ keV, the S factor is approximated by a Breit-Wigner expression using the parameters of the 9-keV resonance: E_R=10±2 keV, $\sigma_r=(2.07\pm0.40)\times10^{-14}$ μb, and Γ_{tot} =15±1 keV. A smooth extrapolation was used to connect the Breit-Wigner curve to the present result. The experimental data for the low proton energy region as well as the fitted line are presented in Fig. 11. The total S factor, obtained in the present experiment, was defined as the sum of the S factors of all primary transitions involved except the transition to the fourth excited state which was neglected due to its very small contribution (less than 1%). Typical values of the present results, obtained by summing the S factors as given in Table I, are shown (along with their uncertainties), at four energies in Fig. 11. In the energy range $80<E_p<170$ keV, even the S factor to the second excited state from the original data [4] is larger than the total S factor adopted in Ref. [22]. For this reason the NACRE data from $80<E_{\text{c.m.}}<170$ keV were excluded from the present fit. Above 170 keV, the nonresonant data from Refs. [20] and [4] were adopted. They

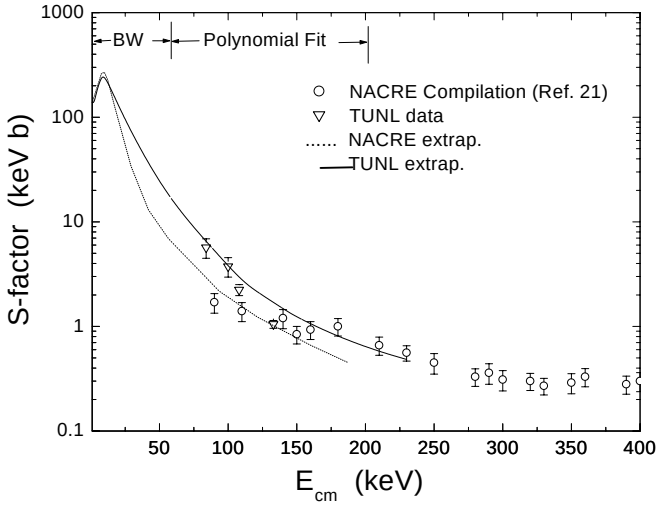

FIG. 11. Total S factor for $^{10}B(p, \gamma)^{11}C$ reaction. The present experimental data (△) are presented simultaneously with the experimental data (○) from Ref. [4]. The solid line is the result of the Breit-Wigner function joined smoothly to polynomial fit to the experimental data described in the text.

cover the reaction rate region from 170 keV to 17 MeV. The S factor in this energy region was represented using a polynomial fit to the data set from Refs. [20] and [4], which was matched smoothly to the S factor curve used at and below 170 keV.

The upper limit E_{max} for the integration was given by the highest energy investigated (E_p=17 MeV) [20]. The lower limit of the integral is E=0. The reaction rate was obtained by numerical integration of the total S factor curve using the expression

$$N_A\langle\sigma\nu\rangle = N_A\frac{(8/\pi)^{1/2}}{\mu^{1/2}(k_BT)^{3/2}}\int_0^{E_{max}} S(E)\exp\left(-\frac{E}{k_BT}-2\pi\eta\right)dE, \tag{14}$$

where μ is the reduced mass, k_B is the Boltzmann constant, and η is the Sommerfeld parameter defined by Eq. (4); E is the particle energy in the center-of-mass system, T is the plasma temperature in K, and μ is the relative velocity of the nucleus and the proton. As in Ref. [21] the evaluation of Eq. (14) was performed using a numerical integration technique in order to calculate the value of the integral to a high degree of accuracy. Regions of fast variation in the integral are automatically subdivided into smaller subregions and integrated separately to minimize the error in the quadrature. Peak value of the E_R =10 keV resonance also included in the energy range of integration. The resulting rates were fit by the analytic expression

$$\begin{aligned}\log_{10}(N_A\langle\sigma\nu\rangle) = {} & 4.52\times10^6/T^{2/3}\exp(-12.064/T^{1/3})/[(T^{2/3} \\ & -0.0295)^2 - 1.28\times10^{-4}](1-1.23T \\ & +1.74T^2-0.299T^3+0.0161T^4),\end{aligned} \tag{15}$$

where the reaction rate is given in units of cm^3 mol^{-1} s^{-1} and $x=\log_{10}(T_9)$. T_9 is the plasma temperature in units of 10^9K. The total error of the fit is 15%.

At very low temperatures ($T_9<0.01$) and relatively higher temperatures ($T_9>1$), the present reaction rate is identical with the latest NACRE compilation [22]. The difference appears between these two regions, where the largest contribution to the integral in Eq. (15) comes from energies between $E_{c.m.}$=20–170 keV. The present experimental S-factor data in this energy range exceed the data used in the NACRE compilation by a factor of 2.6. However, it has to be mentioned that despite this discrepancy, the original differential S-factor data presented in Fig. 6 of Ref. [4] are in good agreement with the present experimental results.

VII. CONCLUSION

In the present work the astrophysical S factors for the $^{10}B(p, \gamma)^{11}C$ reaction have been determined for the three strongest transitions: capture to the ground state, to the second exited state, and to the fifth excited states of ^{11}C. The experiments were performed by measuring simultaneously the number of γ rays, integrated over the thick-target yield curve, coming from (p, γ) and $(p, \alpha\gamma_1)$ reactions.

The present study of the reaction $^{10}B(\vec{p}, \gamma)^{11}C$ at $E_{c.m.}$ =91–145 keV found a substantial vector analyzing power at 90 deg for capture to the ground state, indicating a significant p-wave component. The results of the present measurements show that $A_y(90\text{ deg})=0.32\pm0.03$ at $E_{c.m.}$=145 keV for capture to the ground state of ^{11}C, with smaller values of $A_y(90\text{ deg})$ for the capture to the other excited states. Direct-capture calculations including the known resonances have been performed in an attempt to determine the origin of the p-wave capture strength and its effect on the extrapolation of the astrophysical S factor. The observed analyzing power was explained by considering the subthreshold p-wave ($M1$ radiation) resonance in addition to two high lying $M1$ resonances interfering with the direct-capture plus-resonance s-wave ($E1$) component. The $M1$ strength was adjusted in order to fit both the observed A_y data and the astrophysical S factor data. The spectroscopic factor which is deduced from this strength was found to be C^2S=0.42, compared to the previously determined experimental value of 0.39. Our corrected values of the S factor for the $^{10}B(\vec{p}, \gamma)^{11}C$ reaction between 20 and 170 keV differ from the previous NACRE compilations by a factor of 2.6.

ACKNOWLEDGMENTS

The authors would like to thank C. R. Brune for the useful suggestions during the experiment and J. Dunham for providing excellent beams from ABPIS source. We greatly appreciate the help from all the TUNL staff. One of the authors (N.K.) would like to thank the Triangle Universities Nuclear Laboratory and Duke University for their warm hospitality and support during his stay in the United States. He also would like to acknowledge the financial support of the Dutch Organization for Scientific Research (NWO). This work was supported by U.S. DOE Grant No. DE-FG02-97ER41033.

[1] R. M. Chasteler, H. R. Weller, D. R. Tilley, and R. M. Prior, Phys. Rev. Lett. **72**, 3949 (1994).
[2] S. J. Gaff, R. S. Canon, J. H. Kelley, S. O. Nelson, K. Sabourov, E. C. Schreiber, D. R. Tilley, H. R. Weller, and E. A. Wulf, Phys. Rev. C **59**, 3425 (1999).
[3] J. H. Kelley, R. S. Canon, S. J. Gaff, R. M. Prior, B. J. Rice, E. C. Schreiber, M. Spraker, D. R. Tilley, E. A. Wulf, and H. R. Weller, Phys. Rev. C **62** 025803 (2000).
[4] M. Wiescher, R. N. Boyd, S. L. Blatt, L. J. Rybarcyk, J. A. Spizuoco, R. E. Azuma, E. T. H. Clifford, J. D. King, J. Gorres, C. Rolfs, and A. Vlieks, Phys. Rev. C **28**, 1431 (1983).
[5] C. Angulo, S. Engstler, G. Raimann, C. Rolfs, W. H. Schulte, and E. Somorjai, Z. Phys. A **345**, 231 (1993).
[6] S. Cohen and D. Kurath, Nucl. Phys. **A101**, 1 (1967).
[7] C. Angulo, W. H. Schulte, D. Zahnow, G. Raimann, and C. Rolfs, Z. Phys. A **345**, 333 (1993).
[8] T. B. Clegg, Rev. Sci. Instrum. **61**, 385 (1990).
[9] ACF-Metals, The Arizona Carbon Foil Co., Inc., Tucson, AZ.
[10] A. Anttila, J. Einonen, M. Hautala, and I. Forsblom, Nucl. Instrum. Methods **147**, 501 (1977).
[11] J. F. Briesmeister, computer code MCNP Version 4C (Los Alamos National Lab, Los Alamos, 2000).
[12] C. E. Rolfs and W. S. Rodney, *Cauldrons in the Cosmos* (University of Chicago Press, Chicago, 1988).
[13] M. Youn, H. T. Chung, J. C. Kim, H. C. Bhang, and K. H. Chung, Nucl. Phys. **A533**, 321 (1991).
[14] R. G. Seyler and H. R. Weller, Phys. Rev. C **20**, 453 (1979).
[15] H. R. Weller and N. R. Roberson, Rev. Mod. Phys. **52**, 699 (1980).
[16] J. M. Eisenberg and W. Greiner, *Excitation Mechanism of Nucleus* (North-Holland, Amsterdam, 1988).
[17] H. Kitazawa, Triangle Universities Nuclear Laboratory Report No. TUNL-XIX, 1980.
[18] O. Bersillon, Bruyeres-le-Chatel Report No. CEA-N-2037, 1978.
[19] F. Ajzenberg-Selove, Nucl. Phys. **A506**, 1 (1990).
[20] H. M Kuan, M. Hasinoff, W. J. O'Connell, and S. S. Hanna, Nucl. Phys. **A151**, 129 (1970).
[21] S. O. Nelson, E. A. Wulf, J. H. Kelley, and H. R. Weller, Nucl. Phys. **A679**, 199 (1999).
[22] C. Angulo *et al.*, Nucl. Phys. **A656**, 1 (1999).